Lasers in Manufacturing Conference 2017

Mechanical and corrosion properties of thin Hastelloy C-276 plate by pulsed laser welding with filler wire

Guangyi Ma[a],Dongjiang Wu[a,*], Dongdong Wu[a], Mingkai Lei[b]

[a] *Key Laboratory for Precision and Non-traditional Machining Technology of Ministry of Education, Dalian University of Technology, Dalian, 116024, China*

[b] *School of Materials Science and Engineering, Dalian University of Technology, Dalian, 116024, China*

Abstract

To meet the special requirements of Hastelloy C-276 welding in extreme environment, tensile tests and electrochemical corrosion tests of thin Hastelloy C-276 plate by pulsed laser welding with filler wire (LWFW) were carried out. Laser scanning confocal microscope (LSCM) and Energy Dispersive X-ray Spectrometry analysis (EDS) were carried out to study the corrosion mechanisms and the corroded surface element distribution features. The results indicated, the tensile strength of welding joint with a certain positive reinforcement was higher than that of base metal. Also, all tensile tests were broken at the base metal. In the neutral solution, the corrosion resistance of the weld was greater than that of the base metal. However, in the weak acidic solution, the corrosion resistance of the weld and base metal were similar. In both solutions, the intergranular corrosion occurred at the weld, selective corrosion at the base metal, and a Mo-rich passivation film was grown on the surface of the weaker corroded region.

Keywords: Pulsed laser welding; Filler wire; Hastelloy C-276; Mechanical properties; Electrochemical corrosion properties

1. Introduction

The Ni-based Hastelloy C-276 is widely applied in chemical and nuclear industries due to its excellent properties. Thin Hastelloy C-276 plate welding has been employed in the manufacture of nuclear main pump can in the third-generation nuclear power plant by Zheng et al., 2016. Special mechanical and corrosion-resistant properties requirements of Hastelloy C-276 welding are demanded in extreme conditions.

* Corresponding author. Tel.: +86-411-84707625; fax: +86-411-84707625.
E-mail address: djwudut@dlut.edu.cn.

Arc welding, electron beam welding and laser welding had been used to Hastelloy C-276 welding. Li et al., 2011 indicated that many precipitation phases were observed in Hastelloy C-276 by gas tungsten arc welding (GTAW) with ERNiCrMo-4 filler wire, and the tensile strength of weld joint was lower than that of the base metal. Manikandan et al., 2014 reported that, the weld by pulsed current GTAW was found to be better in strength and freedom from micro-segregation and secondary phases. Ahmad et al., 2005 reported electron beam welding process required a vacuum environment. Wu et al., 2013, 2015 found fine grain, low degree of segregation, no obvious brittle phase and great mechanical and corrosion-resistant properties were obtained by pulsed laser welding without filler wire. Laser welding could replace arc welding process as the important means of nuclear main pump can welding due to its low heat input and rapid cooling, but negative reinforcement was easily produced in laser welding without filler wire process, detrimental to the performance of nuclear main pump can.

In this paper, thin Hastelloy C-276 plate pulsed laser welding with filler wire was proposed. Tensile tests and electrochemical corrosion tests of Hastelloy C-276 welding were carried out to meet the requirements of Hastelloy C-276 welding in extreme environment. LSCM and EDS were carried out to study the corrosion mechanisms and the corrosion behavior features.

2. Experiment

In the experiment, 0.5 mm thick Hastelloy C-276 plate (100 mm×40 mm) and 0.5 mm diameter ERNiCrMo-4 filler wire according to AWS A5.11 / A5.14 were employed and their chemical composition were given in Table 1. JK701H pulsed Nd: YAG laser with a focused spot diameter of 0.5 mm and self-improvement wire feeder system were used in welding experiment. The filler wire was supplied at an angle α of 30° with the Hastelloy C-276 plate into the leading edge of the weld pool. 99.9vol. % Argon as shielding gas was used. The LWFW device was shown in Fig. 1(a). According to the previous investigation by Wu et al. 2017, the weld with uniform reinforcements and contact angles on upper and lower surface and free defect could be obtained under the conditions with pulse energy of 1.25 J, pulse duration of 6 ms, pulse frequency of 60 Hz, welding speed and wire feeding speed of 350 mm/min and defocus of -1 mm. The weld cross section was shown in Fig. 1(b).

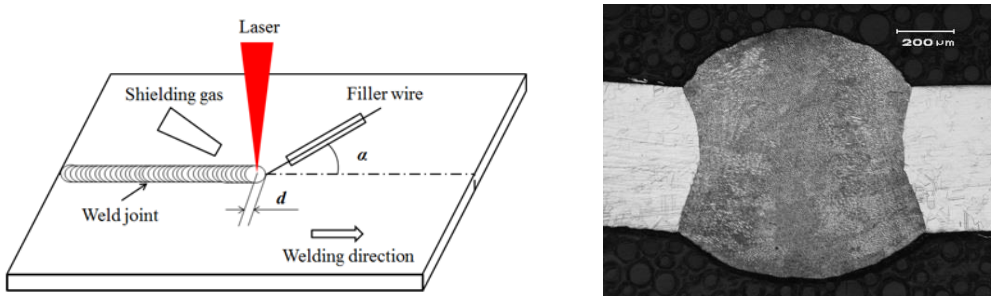

Fig. 1. Laser welding with filler wire (a) experiment device schematic; (b) the weld cross section morphology

Table 1. Chemical composition of Hastelloy C-276 and ERNiCrMo-4 (wt. %)

Samples	Ni	Cr	Mo	Fe	W	Co	Mn	C	Si	P	S	V
Hastelloy C-276	Bal.	16.00	15.58	5.14	3.45	1.26	0.53	0.001	0.02	0.006	0.003	0.01
ERNiCrMo-4	Bal.	16.00	15.20	5.30	3.30	0.11	0.41	0.009	0.03	0.003	0.001	0.01

WDW-50E universal tensile testing machine was used in tensile tests with a constant travel speed of 5 mm/min. The tensile samples were prepared according to GB/T 2651-2008 standard. A three-electrode electrochemical system with a saturated calomel reference electrode and a Pt plate counter electrode, together with an electrochemical system PARSTAT 2273, was used for the potentiodynamic polarization measurements. The weld samples, working electrode, were cut along the weld longitudinal direction at the mid of the weld. The would-corroded area of the weld and base metal samples were ground sequently and polished. Before the corrosion tests, the samples were insulated by the insulating gel except the would-corroded area. Neutral (3wt. % NaCl) and weak acidic (3wt. % H_3BO_3, 3 g NaCl was added per 100 mL of H_3BO_3 solution to increase the solution conductivity) solutions were applied as corrosion solution according to the actual service conditions of nuclear main pump can. Each specimen was scanned potentiodynamically at scan rate 5 mV/s, from -0.5 V to 1.5 V. After the corrosion tests, the corroded surface morphology and element distribution features were observed by LSCM and EDS.

3. Results and discussion

3.1. Mechanical properties

Table 2 showed the tensile test results of the base metal and weld joint. It was found that the yield strength (YS) of base metal and weld joint did not show a significant difference, and the ultimate tensile strength (UTS) of the weld joint was greater than that of the base metal, and all the fractures of the weld joints happened at the base metal as shown in Fig. 2. The analysis showed that due to fine grain strengthening from the Hall-Petch relation, the yield strength of the weld with finer grain was improved. However, the original solid solution strengthening of base metal was destroyed during the welding process, The combination of the above two effects made the YS of the weld joint and base metal were similar. Due to the rapid cooling of the welding process a large number of unbalanced vacancy defects in the weld could be produced, resulting in dislocation accumulation and stress concentration during tensile tests (Wu et al., 2015). But the weld with a certain positive reinforcement was generated after laser welding with filler wire. The maximum thickness of the weld was approximately 1.8 times that of the base metal, and the average minimum equivalent tensile stress (ETS, representing the actual tensile stress of the weld at the maximum thickness position when fractured) was about 486 MPa, which was only 56.7% of the UTS of the base metal. It could be seen that the tensile properties of the weld joint with a certain positive reinforcement were better than that of base metal.

Table 2. Results of tensile tests

Samples	YS/Average (MPa)		UTS/Average (MPa)		ETS/Average (MPa)		Fracture
	406		861		———		———
Base metal	407	Ave. 406	854	Ave. 857	———		———
	405		856		———		———
	410		862		479		Base metal
Weld joint	409	Ave. 412	877	Ave. 875	487	Ave. 486	Base metal
	418		886		492		Base metal

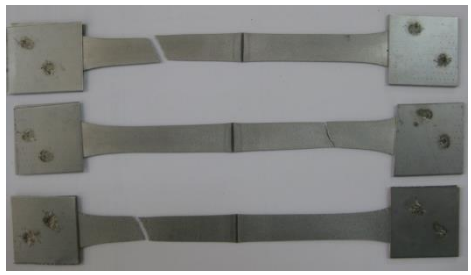

Fig. 2. Tensile samples of the weld

3.2. Electrochemical corrosion characteristics in the neutral solution

Fig. 3 showed the electrochemical corrosion polarization curves of the Hastelloy C-276 weld and the base metal at a 3wt. % NaCl solution. According to the section of less than 0 V of the polarization curves, the Tafel extrapolation method was used to obtain the corrosion potential E_{corr} and the corrosion current density I_{corr} of the weld (WM) and the base metal (BM). It was found that the E_{corr} of the weld (-186.187 mV) was slightly higher than that of the base metal (-278.358 mV), And the I_{corr} of the weld (1.444×10^{-7} A/cm^2) was only about half of that of the base metal (3.485×10^{-7} A/cm^2). According to the corrosion thermodynamics decided by the E_{corr}, the corrosion trend of the weld was weaker than that of the base metal, however according to the corrosion kinetics decided by the I_{corr}, the corrosion rate of the weld was slower than that of the base metal. In the section of 0 to 1.0 V of the polarization curves, obvious passivation transition characteristics and typical stable passivation characteristics were not found in both the weld and the base metal. However, according to the changing trend of current density, it was still considered that there were still a certain passivation in the base metal and the weld. In the sections of more than 1.0 V, the curve of the weld showed the same trend as that of the base metal, showing a certain over-passivation characteristics. In summary, it was found, in the neutral solution, the corrosion resistance of the weld by laser welding with filler wire was better than that of the base metal.

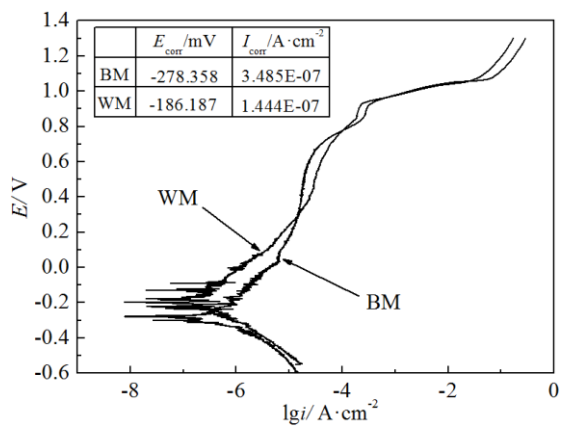

Fig. 3. Polarization curves in NaCl solution

For in-depth analysis of the corrosion mechanism in the neutral solution, the corroded surface morphology of the base metal and the weld was observed by LSCM, as shown in Fig. 4 and Fig. 5,

respectively. It could be seen from Fig. 4 that obvious selective corrosion were observed in the base metal. Wider and narrower stripe features could be seen on the corroded surface. The contour size of the wider stripe was similar to the grain average size of the base metal (40~60 μm). This was mainly related to the slightly difference of element distribution and atoms irregular arrangement and loose structures at grain boundary. The narrower stripe feature, whose contour size had a lager difference with the average grain size of the base metal, may be related to the sub-grain boundaries which were prone to occur in Ni-based alloys. Form Fig. 5, intergranular corrosion was observed in the weld, which was related to the micro-segregation and atoms irregular arrangement and loose structures at grain boundary. The maximum roughness difference (nearly 3 μm) on base metal surface was much higher than that on the weld surface (less than 1 μm). All above, it could be concluded, the base metal showed the selective corrosion mechanism, but in the weld the intergranular corrosion was the primary corrosion mechanism in the neutral solution.

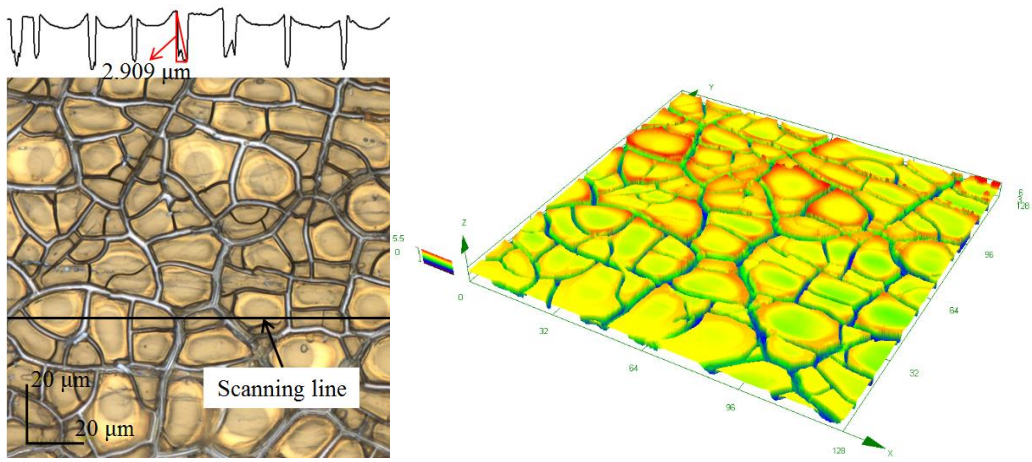

Fig. 4. Corroded surface morphology of base metal in NaCl solution

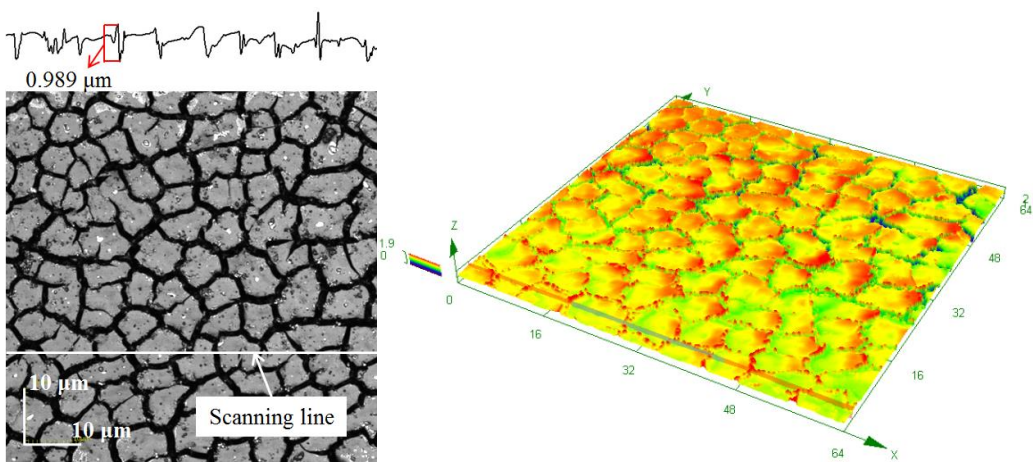

Fig. 5. Corroded surface morphology of the weld in NaCl solution

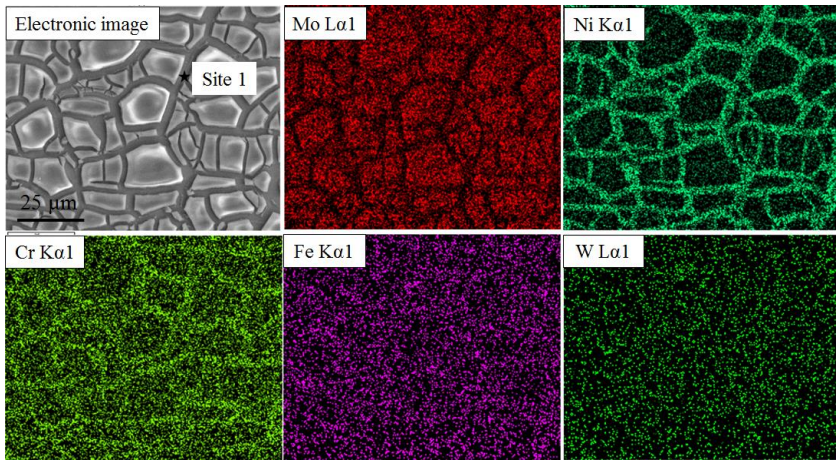

Fig. 6. Element distribution of base metal corroded surface in NaCl solution

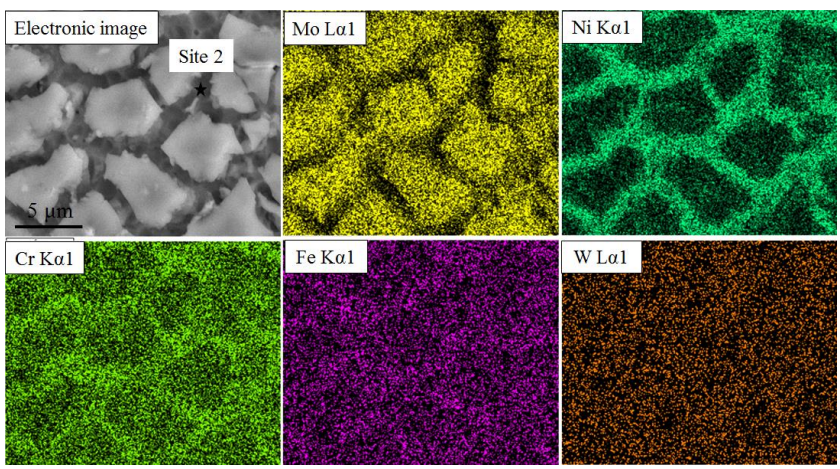

Fig. 7. Element distribution of the weld corroded surface in NaCl solution

In order to confirm the electrochemical corrosion behavior in the neutral solution, the corroded surface element distributions of the base metal and the weld were observed by EDS, as shown in Fig. 6 and Fig. 7, respectively. Combined with the characteristics of corrosion morphology, it was found, element distribution characteristics on the corroded surface of the base metal and the weld were similar. The contents of Ni and Cr in the corroded stripes were higher than those in the weaker corroded region (grain body). The element distributions in the corroded stripes (site 1 of the base metal in Fig. 6: Mo: 14.28 %, Cr: 16.11 %, Fe: 5.55 %, W: 3.52 %, Co: 1.25 %, Ni: bal.; site 2 of the weld in Fig. 7: Mo: 14.74 %, Cr: 16.00 %, Fe: 5.82 %, W: 3.92 %, Co: 0.75 %, Ni: bal.; mass fraction) were similar with that in the equiaxed dendritic region of the uncorroded base metal and weld. In the weaker corroded region of both the base metal and the weld, Mo element content was much higher than its average content in the base metal and the weld. Fe and W element distributions were uniform in different regions. Those were mainly related to that the passivation trend of Cr and Mo was stronger than that of Ni and Fe, which were favorable for the formation of stable passivation

films such as Cr_2O_3 and MoO_4^{2-}. However, due to the atoms irregular arrangement, loose structures and high interface energy at the grain and sub-grain boundary, Cl^- in the corrosion solution easily reacted with the grain and sub-grain boundary metal to form a soluble compound, which had a certain destructive effect on the passivation film, and formed the corroded surface fringe profile.

3.3. Electrochemical corrosion characteristics in the weak acidic solutions

Fig. 8 showed the polarization curves of the Hastelloy C-276 weld and the base metal at a 3wt. % H_3BO_3 solution. E_{corr} and I_{corr} of the weld (WM) and the base metal (BM) could be obtained by Tafel extrapolation method in the section of less than 0 V of the polarization curves. It was found that the E_{corr} and I_{corr} of the weld(-269.262 mV and 1.067×10^{-6} A/cm^2, respectively) were similar with those of the base metal (-273.383 mV and 1.831×10^{-6}A/cm^2, respectively). The corrosion trend and corrosion rate of the weld and the base metal were similar from the corrosion thermodynamics and kinetics. In the sections of more than 0 V, Obvious passivation transition and typical stable passivation characteristics were not found in both the weld and the base metal. However, according to the changing trend of current density, it was still considered that a certain passivation occurred in the weld and base metal. After 0 V, the curve of the weld showed the same trend as that of the base metal. In summary, in the weak acidic solution, the corrosion resistance of the weld by laser welding with filler wire was similar with that of the base metal.

The corrosion mechanism of the base metal and the weld in the weak acidic solution were studied by observing the corroded surface morphology using LSCM, as shown in Fig. 9 and Fig. 10, respectively. From Fig. 9, obvious selective corrosion mechanism with wider and narrower stripe features on the corroded surface was observed in the base metal. It was mainly related to the slightly difference of element distribution, atoms irregular arrangement and loose structures at grain boundary and sub-grain boundaries. Form Fig. 10, intergranular corrosion was observed in the weld, which was related to the micro-segregation and irregular arrangement of atoms and loose structures at grain boundary. The maximum roughness difference (higher than 3 μm) on base metal surface was much higher than that on the weld surface (less than 1 μm). All above, base metal showed the selective corrosion mechanism but the weld the intergranular corrosion in the weak acidic solution, which were similar with the corrosion mechanisms in the neutral solution.

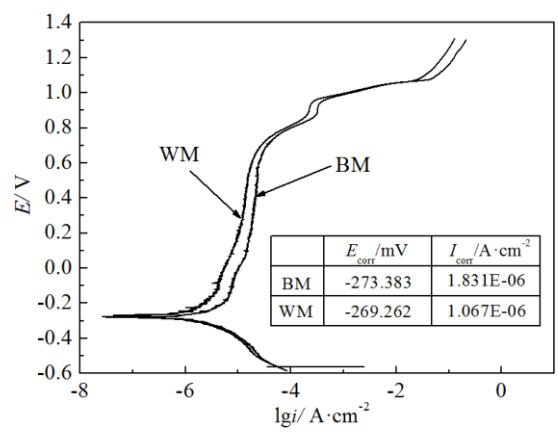

Fig. 8. Polarization curves in H_3BO_3 solution

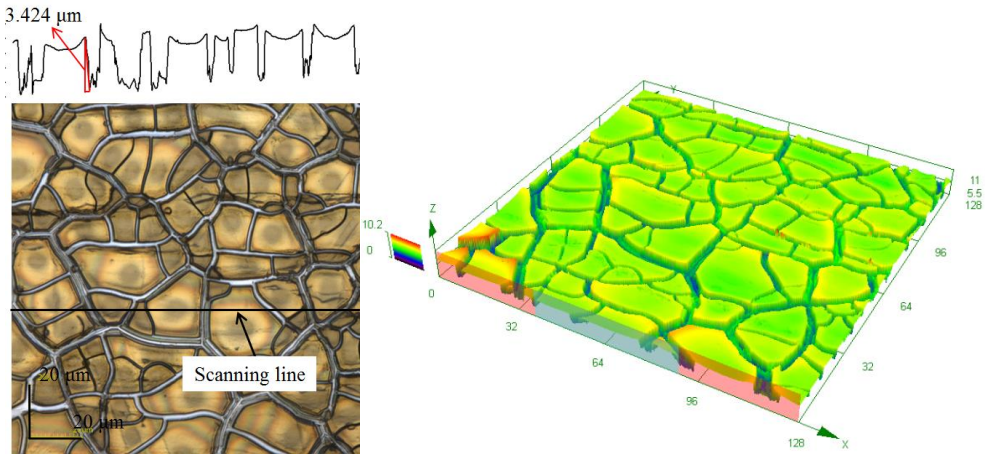

Fig. 9. Corroded surface morphology of base metal in H_3BO_3 solution

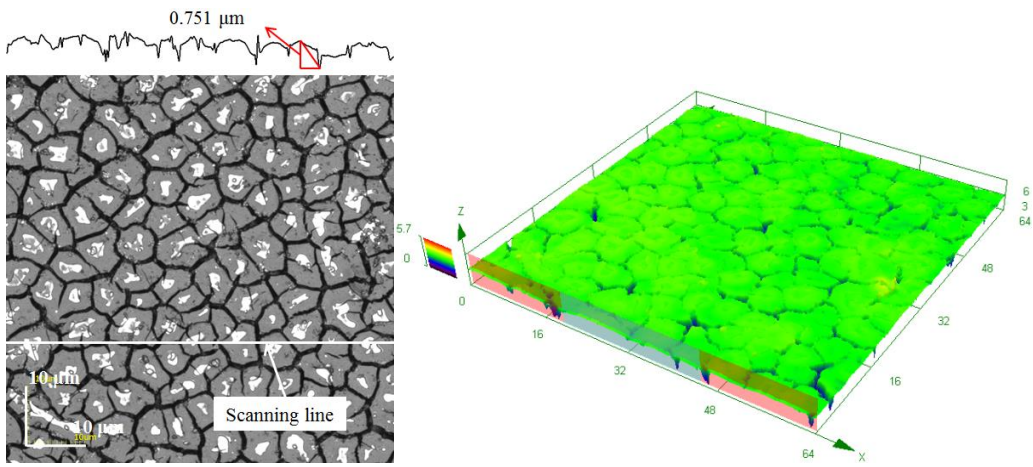

Fig. 10. Corroded surface morphology of the weld in H_3BO_3 solution

To confirm the electrochemical corrosion behavior in the weak acidic solution, element distribution of the base metal and the weld corroded surface were observed by EDS, as shown in Fig. 11 and Fig. 12, respectively. Combined with the corrosion morphology characteristics, element distribution characteristics on the corroded surfaces of the base metal and the weld were similar. The contents of Ni and Cr in the corroded stripes were higher than those in the weaker corroded region (grain body). The element distribution in the corroded stripes of the weld (site 2 in Fig. 12: Mo: 16.12 %, Cr: 16.17 %, Fe: 5.66 %, W: 3.64 %, Co: 0.89 %, Ni: bal.; mass fraction) was similar with that in the equiaxed dendritic region of the uncorroded weld. However, according to site 1 in Fig. 11 (Mo: 10.29 %, Cr: 16.68 %, Fe: 5.68 %, W: 3.62 %, Co: 1.24 %, Ni: bal.; mass fraction), the content of Mo in the corroded stripes of the base metal was lower than Mo average content of the base metal. In the weaker corroded region of the base metal and the weld, Mo element content was much higher. Fe and W element distribution were uniform in different regions. Those were mainly related to that the passivation trend of Cr and Mo was stronger than that of Ni and Fe,

which was favorable for the formation of stable passivation films such as Cr_2O_3 and MoO_4^{2-}. However, due to the atoms irregular arrangement, loose structures and high interface energy at the grain and sub-grain boundary, Cl^- had a certain destructive effect on the passivation film at the grain and sub-grain boundary.

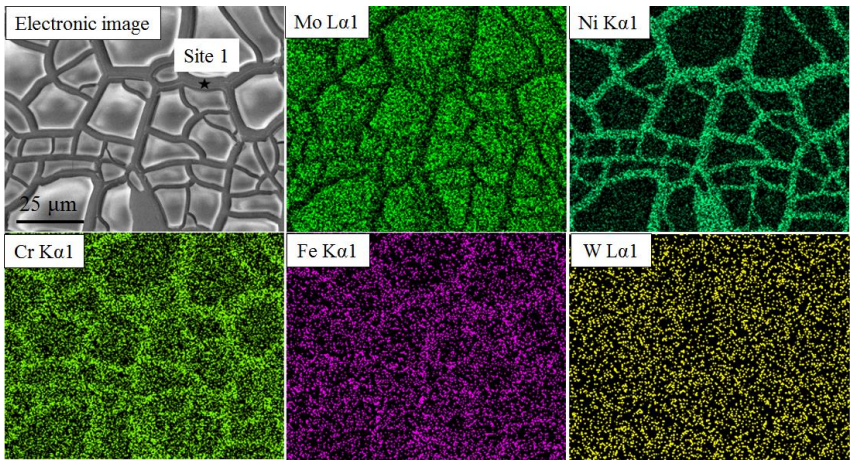

Fig. 11. Element distribution of base metal corroded surface in H_3BO_3 solution

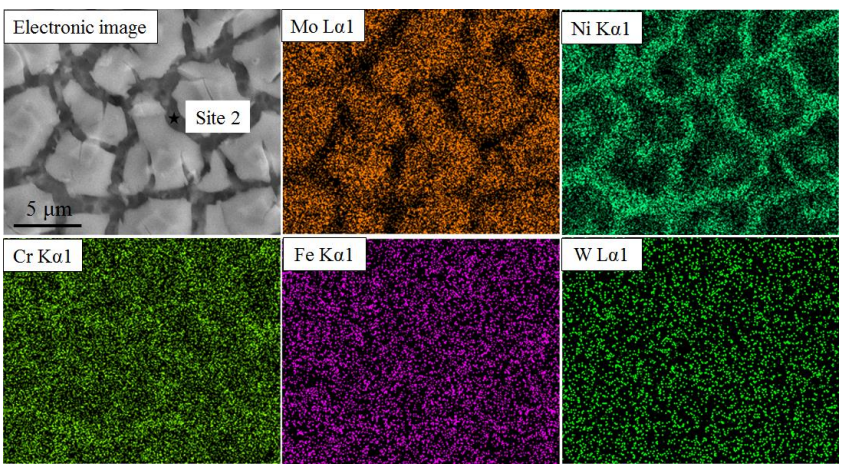

Fig. 12. Element distribution of the weld corroded surface in H_3BO_3 solution

4. Conclusion

In the present work, tensile and electrochemical corrosion properties of Hastelloy C-276 by pulsed laser welding with filler wire were evaluated. The conclusions are summarized below.

(1) The average minimum ETS of the weld joint was only about 56.7% of the UTS of the base metal. All the fractures of the weld joints happened at the base metal and the tensile properties of the weld joint with a certain positive reinforcement were better than that of the base metal.

(2) In the neutral solution, the corrosion resistance of the weld was better than that of the base metal. The base metal showed the selective corrosion mechanism. But the intergranular corrosion was the primary

corrosion mechanism of the weld. In the grain body of the base metal and the weld, stable passivation films enriched Mo were generated, preventing the metal from being corroded.

(3) In the weak acidic solution, the corrosion resistance of the weld was similar with that of the base metal. The base metal showed the selective corrosion mechanism but the weld the intergranular corrosion, which were similar with the corrosion mechanisms in the neutral solution. In the grain body of base metal and the weld, stable passivation films enriched Mo were generated.

Acknowledgements

This research was supported by the National Key Basic Research Program of MOST of P.R. China (Grant No. 2015CB057305).

References

Ahmad, M., Akhter, J. I., Akhtar, M., Iqbal, M., Ahmed, E., Choudhry, M. A., 2005. Microstructure and hardness studies of the electron beam welded zone of Hastelloy C-276. Journal of Alloys and Compounds, 390(1), pp. 88-93.

Li, X., Yan, Y., Liu, Y., He, X., 2011. Study on microstructure and properties of welded joint of extra thin Ni-based alloy plate. Journal of Plasticity Engineering, 06, pp. 91-96.

Ma, G., Niu, F., Wu, D., Qu, Y, 2013. Electrochemistry corrosion properties of pulsed laser welding Hastelloy C-276. Physics Procedia, 41, pp. 31-37.

Ma, G., Wu, D., Niu, F., Zou, H, 2015. Microstructure evolution and mechanical property of pulsed laser welded Ni-based superalloy. Optics and Lasers in Engineering, 72, pp. 39-46.

Manikandan, M., Arivazhagan, N., Rao, M. N., & Reddy, G. M., 2014. Microstructure and mechanical properties of alloy C-276 weldments fabricated by continuous and pulsed current gas tungsten arc welding techniques. Journal of Manufacturing Processes, 16(4), pp. 563-572Zheng, M., Yan, J., Jun, S., Tian, L., Wang, X., Qiu, Z., 2016. The general design and technology innovations of CAP1400. Engineering, 2(1), pp: 97-102.

Manikandan, M., Hari, P. R., Vishnu, G., Arivarasu, M., Ramkumar, K. D., Arivazhagan, N., Reddy, G. M., 2014. Investigation of Microstructure and Mechanical Properties of Super Alloy C-276 by Continuous Nd: YAG laser Welding. Procedia Materials Science, 5, PP. 2233-2241.

Wu, D., Chai, D., Ma, G.,Zhou, S., Yu, J., Wu, D., 2017. Effect of pulsed laser welding with filler wire on weld forming and microstructures of thin Nickel based alloy sheet. Laser & Optoelectronics Progress, 54, P. 031404.